RSC Advances

PAPER

View Article Online
View Journal | View Issue

Cite this: *RSC Adv.*, 2026, **16**, 4432

Impact of calcium, zinc or aluminum dimethylphosphate coordination polymers on flame retardancy and rheological properties of poly(butylene succinate)

Mateusz Kullas, *[a] Maciej Dębowski, [b] Paweł Groch, [a] Anna Czajka-Warowna [c] and Krystyna Czaja [a]

In this paper the impact of three metal diorganophosphates (MtDOPs) coordination polymers: calcium bis(dimethyl phosphate) (CaDMP), zinc bis(dimethyl phosphate) (ZnDMP) and aluminum tris(dimethyl phosphate) (AlDMP) on the flame retardancy and rheological properties of poly(butylene succinate) (PBS) is discussed in detail. The incorporation of 20 wt% of MtDOPs into PBS improved self-extinguishing properties, since all investigated composites achieved a V-2 rating in the UL-94 test. In the limited oxygen index (LOI) test the best effect was demonstrated by CaDMP, which enhanced the LOI value from 23.6 vol% for neat PBS to 27.3 vol% for PBS/20%CaDMP. We also found that AlDMP effectively suppressed melt-dripping in UL-94 and LOI tests due to a strong increase in complex viscosity and the existence of a relative high apparent yield stress for the PBS/20%AlDMP composite, which we observed in the rheological tests. In the mass loss calorimeter (MLC) test, MtDOPs reduced peak heat release rate (pHRR), total heat evolved (THE) and enhanced char yield (CY). The best result is offered by ZnDMP, in which case pHRR and THE decreased by 57 and 24%, respectively. Based on MLC test results, solid residue characterization as well as evolved gas analysis by means of thermogravimetry coupled with FTIR spectroscopy, the possible flame retardancy mechanism of MtDOPs in PBS was proposed. MtDOPs improve the fire response of PBS acting in the gas phase by liberating trimethyl phosphate (TMP) and in the condensed phase by increasing CY. Formation of a foamed and compact char acting as a barrier for heat and mass transport was also observed during combustion of a ZnDMP-containing composite.

Received 8th September 2025
Accepted 6th January 2026

DOI: 10.1039/d5ra06774j

rsc.li/rsc-advances

1 Introduction

The growing environmental awareness, problems with plastic waste disposal, as well as depletion of fossil resources have impact for dynamic development of biodegradable and/or bio-obased polymers. Such polymers, including their composites, are also of considerable interest to the scientific community. Among the synthetic, thermoplastic and biodegradable polymers, PBS has attracted attention over the least years. The monomers for its synthesis, succinic acid and 1,4-butanediol can be derived from petroleum oil, or from renewable sources *via* a fermentation route using cellulose as the primary raw material.[1,2] PBS due to its easy processing and good mechanical properties, is a candidate for replacing widely used petrochemical-based and non-compostable polyethylene and isotactic polypropylene (iPP).[1,3,4]

Unfortunately, due to the poor fire resistance of PBS, its application is heavily restricted in such sectors as electrical and electronics, automotive, construction *etc.* Neat PBS exhibits relatively low value of limited oxygen index (LOI) – 21.0–24.0 vol%[3] and does not achieve a rating in the vertical UL-94 test even at 3.2 mm thickness.[3,5] One way to improve the fire performance of PBS is the incorporation of additives, preferably halogen-free flame retarders. In contrast to easy-to-synthesise and cheap metal hydroxides, the phosphorus-containing flame retardants are significantly much effective in terms of fire retardancy. As reported by Wang *et al.*, a PBS composite containing 25 wt% aluminum diethylphosphinate (AlPi), with PBS-grafted-maleic acid acting as a compatibilizer, achieved a V-0 rating in the UL-94 test at a thickness of 3.2 mm, demonstrating LOI of 29.5 vol%.[6] Melamine phosphate (MP), melamine phosphite (MPi) and melamine hypophosphite (MHP) at 30 wt% loading, also lead to the same UL-94 rating (V-0 at 3.0 mm) accompanied by LOI value of 28.0 vol%, 30.5 vol%, 29.0 vol% respectively.[7] Similar results

[a]*Institute of Chemistry, Opole University, Oleska 48, 45-052 Opole, Poland. E-mail: mateusz.kullas@gmail.com*

[b]*Faculty of Chemistry, Warsaw University of Technology, Noakowskiego 3, 00-664 Warsaw, Poland*

[c]*Faculty of Materials Science and Engineering, Warsaw University of Technology, Wołoska 141, 02-507 Warsaw, Poland*

have been obtained *via* incorporation of a common commercial flame retarder, namely ammonium polyphosphate (APP). In such a case, PBS composite is characterized with the V-0 rating (at 3.0 mm) at a loading of 30 wt% of APP and LOI value of 33.3 vol%.[8]

In a recent paper we have reported on the positive effect of three polymeric MtDOPs: $Ca[O_2P(OCH_3)_2]_2$ (CaDMP), $Zn[O_2P(OCH_3)_2]_2$ (ZnDMP) and $Al[O_2P(OCH_3)_2]_3$ (AlDMP) on the flammability of iPP.[9] All studied composites containing 20 wt% of these compounds reached V-2 rating in UL-94 test and exhibited LOI value of 25.5 vol%, 21.2 vol%, 21.6 vol% for CaDMP, ZnDMP and AlDMP-containing system, respectively.

It is widely known that the same chemical compounds can exhibit a completely different flame retardant efficiency depending on the polymer matrix into which they are incorporated. Li *et al.* in their comparative study reported on a very good flame retardancy effect of AlPi dispersed in poly(2,6-dimethyl-1,4-phenylene oxide) (PPO) and only a moderate one in iPP-based composite: with an addition of 30 wt% of AlPi into PPO matrix a significant increase of LOI value from 29.0 vol% to 43.0 vol% was determined, whereas the same AlPi loading in iPP increased LOI from 17.0 vol% to *ca.* 26.0 vol%. Even greater differences in the fire response were recognized in cone calorimeter tests. For PPO/30%AlPi composite, the pHRR was reduced by 72% with respect to neat PPO, while iPP/30%AlPi composite showed pHRR value higher by 9% compared to the unmodified iPP sample. Such various impacts of AlPi on the flammability of PPO and iPP was found to be attributable to the differences in a mode of action of AlDPi. In both polymers, AlPi acts in the gas phase decreasing the avEHC value of the volatiles, but only in PPO-based system AlPi is also active in the condensed phase as exhibited by the formation of thick, relatively dense and strong char structures that constitute an additional protective barrier for heat and mass transfer.[10] Similar differences in fire resistance were recorded in the case of poly(lactic acid) (PLA) and iPP modified with APP. It was found that the presence of 20 wt% of APP suppressed dripping and effectively improved the fire performance of PLA in the vertical UL-94 test (the resulting composite achieved V-0 rating at 4.0 mm thickness). In turn, at the same APP loading the composite based on iPP as polymer matrix exhibited dripping behaviour and did not achieve a rating in UL-94 test.[11]

Therefore, although CaDMP, ZnDMP, and AlDMP demonstrate good flame-retardant performance in fully hydrocarbon polymer such as iPP, this does not mean that a similar behavior will be gained by other polymer systems. In particular, predicting the flame-retardant effectiveness of MtDOPs in polymers with chemical structures that prove significantly different from iPP poses a challenge. It was the motivation to continue the investigations and to examine the CaDMP, ZnDMP and AlDMP as possible flame retardants for heteroatom-contained and biodegradable PBS. To the best of our knowledge, this is a first literature report concerned with the improvement of fire performance of heteroatom-contained, thermoplastic polymer by the utilization of CaDMP, ZnDMP or AlDMP.

2 Experimental

2.1 Materials

PBS with 51% of biobased carbon (PBE 003, Melt Flow Index of 5 $\pm$ 1 g 10 min^{-1} at 190 °C and 2.16 kg, density 1.26 g cm^{-3}) was provided by NaturePlas. CaDMP, ZnDMP and AlDMP were synthesized according to the procedures described in previous papers, which also reports on the details of their physicochemical properties.[12–15]

2.2 Preparation of the PBS-based composites

Prior to their usage, PBS granulates were dried at 90 °C for 4 h to remove the residual water and later processed. PBS-based materials containing 20 wt% of the respective MtDOP were prepared by the melt blending method using a HAAKE PolyLab Rheomether (Thermo Fisher Scientific) working for 6 min at 135 °C and 80 rpm. In order to obtain the specimens for the UL-94 and MLC tests, the granulates of the investigated materials were pressed at 135 °C into 2.1 mm thick plates using a QC677A hand press (Comatech). The specimens for LOI and rheological investigations were obtained using an IM-15 laboratory twin screw extruder (processing conditions: 145–160 °C, 100–200 rpm) coupled with an IMM-15 laboratory injection machine (processing conditions: 160 °C, 7 MPa, form temperature of 50 °C) (ZAMAK). Hereinafter, the obtained composites will be denoted as PBS/20%MtDOP.

Samples of the reference material (neat PBS) were obtained using the same procedures as previously described.

2.3 Self-extinguishing tests

LOI and vertical UL-94 tests were used to study the self-extinguishing properties of the obtained materials. The LOI test was carried out according to the ISO 4589 standard using a FTT apparatus (Fire Testing Technology Ltd). The test specimens were bar-shaped with dimensions of 80 mm $\times$ 10 mm $\times$ 4 mm. The vertical UL-94 tests was carried out according to the ISO 60695-11 standard using 125.0 mm $\times$ 13.0 mm $\times$ 2.1 mm specimens.

2.4 Rheological test

Rheological properties of the injection-moulded samples were investigated with a Discovery Hybrid Rheometer HR20 (TA Instruments). The rheometer was equipped with environmental test chamber and parallel plates (diameter of 25 mm, gap of 1 mm). In order to ensure the highest quality of the obtained results, a temperature gap correction was carried out. The existence and extent of the linear viscoelastic regime was determined by measuring the dynamic storage $G'(\omega)$ and loss $G''(\omega)$ moduli, as a function of strain at 6.28 rad s^{-1}. For the frequency sweeps the maximum strain within the linear region for each frequency was used. The rheological measurements were carried out in between 170 and 210 °C, and the temperature range was adjusted to match the melting temperature of the samples. The temperature was maintained within $\pm$0.2 °C. The experimental protocol consisted of heating the rheometer

to a predetermined temperature, holding isothermally for 15 min to equilibrate and then setting the gap separation. Before each measurement a fresh sample was loaded in the preheated rheometer and held for 6 min to allow for thermal equilibrium.

2.5 Mass loss calorimeter test

The burning behaviour under forced flaming conditions was characterized using a MLC (Fire Testing Technology Ltd) according to ISO 13927 standard at the external heat flux of 50 kW m^{-2}. The test specimens had dimensions of 100.0 mm × 100.0 mm × 2.1 mm. For each material, the reported parameters are the average of three measurements.

2.6 Morphological and elemental analysis

A scanning electron microscope (SEM) TM3000 (Hitachi) was used to determine the morphology of PBS/20%MtDOPs, as well as solid residues obtained from the combustion of these materials in MLC. The samples were fixed on the aluminium sample stubs and coated with silver by conventional sputtering techniques. The employed accelerating voltage was 15 kV.

The analysis of the phosphorus to metal molar ratio in MtDOPs, as well as in the char residues after combustion of PBS/20%MtDOPs in MLC was performed by energy dispersive X-ray spectroscopy (EDS) using QUANTAX 70 system. For each sample, the reported phosphorus to metal molar ratio are the average of ten measurements at the accelerating voltage of 15 kV.

2.7 Fourier transform – infrared spectroscopy

FTIR analysis was performed for solid samples crushed with KBr powder and pressed into tablets. The FTIR spectra were recorded with a Nicolet Nexus 2002 FTIR spectrometer (Thermo Fisher Scientific) over a spectral range of 4000–400 cm^{-1} at a resolution of 2 cm^{-1}.

2.8 Raman spectroscopy

Raman spectra were collected on a Nicolet Almega XR spectrometer equipped with a 532 nm laser (Thermo Fisher Scientific) from 4000 to 400 cm^{-1} with the 2 cm^{-1} resolution (exposition time of 4 s, 10 expositions).

2.9 Thermogravimetry coupled with infrared spectroscopy

Thermal degradation was investigated using a combined thermogravimetry coupled with infrared spectroscopy analysis (TGA–FTIR). On-line analyses of the gases evolved during pyrolysis were performed using a Nicolet 6700 FTIR spectrometer (Thermo Electron Corporation) connected to a TGA Q500 apparatus (TA Instruments). The tested samples (8.8 ± 1.4 mg) were placed in platinum pans and heated under nitrogen (a flow rate of 90 mL min^{-1}) from room temperature to 480 °C at a heating rate of 10 °C min^{-1}. In order to allow the decomposition products in a gaseous state, the connections for gas transportation between TGA and FTIR instruments were maintained at 240 °C, whereas the temperature of FTIR gas cell was set at 250 °C. FTIR spectral data were collected as the sum of 32 scans performed every 7 s over the spectral range 600–4000 cm^{-1}.

3 Results and discussion

3.1 LOI and UL-94 performance

The first step in the characterization of the flame retardancy of neat PBS and obtained PBS/20%MtDOPs materials were investigations of the self-extinguishing properties using the LOI and vertical UL-94 tests – the obtained results are shown in Table 1, whereas the digital photos of the samples subjected to LOI test are shown in Fig. 1.

Neat PBS has the LOI value of 23.6 vol% and does not achieve a UL-94 rating, as it exhibits dripping and melt flow in both tests (Fig. 1a). LOI value remained the same after incorporation of the AlDMP particles into PBS, while for ZnDMP- and CaDMP-containing materials it increased to 25.1 vol% and 27.3 vol%, respectively. We should note that MtDOPs had more positively impact on LOI values of analogous composites with iPP. This was particularly evident in the case of AlDMP, which, when introduced into the iPP matrix at 20 wt%, results in a 3.8 vol% increase in LOI.[9] Moreover, all PBS/20%MtDOPs were rated as the V-2 class materials in the UL-94 test and their average total afterflame times were significantly decreased, when compared to that of neat PBS (Table 1). Similar to neat PBS, samples containing CaDMP or ZnDMP flowed and dripped when subjected to the UL-94 test. In contrast, the PBS/20%AlDMP composite exhibited the detachment of partially charred solid fragments; in all cases, the falling liquid droplets or solid fragments led to cotton ignition. In the LOI test after ignition of a neat PBS, PBS/20%CaDMP and of PBS/20%ZnDMP the heat released in the flame induced formation of the polymer droplets running down the edges of the samples (Fig. 1a–c). In addition, for PBS/20%ZnDMP an intensive foaming in the burning front and subsequent flowing down of some of the newly-formed foam was observed (Fig. 1c). It should be noted that for the composites with 20 wt% of CaDMP or ZnDMP, as well as for a neat PBS burned length exceeding 50 mm was applicable as a cut-off criterion in measurement of LOI. On the contrary, AlDMP taking in the dosage of 20 wt% effectively suppresses melt flow and dripping during LOI test (Fig. 1d) and, as a consequence, the cut-off criterion referring to the burning time > 180 s was applied for the PBS/20%AlDMP composite.

It is worth noting that regarding a cut-off criterion in LOI test PBS/20%ZnDMP differs from its iPP-based analogue. For the latter burning time > 180 s was found and indicates more intense flow of PBS/20%ZnDMP than iPP/20%ZnDMP during LOI test.

3.2 Melt rheology studies – dripping correlation

To explain the differences in dripping and melt flow during combustion in LOI and UL-94 test of PBS/20%MtDOPs composites, their rheological properties were assessed. Moreover, the rheological behaviour of polymer melts is crucial for successful processing of thermoplastic polymers by means of

Table 1 Results of LOI and vertical UL-94 tests carried out for PBS and its composites loaded with 20 wt% of MtDOP

	LOI[a]		UL-94		
Sample	(Vol%)	Dripping	Rating	$(t_1+t_2)^b$ (s)	Dripping/ignition of cotton
Neat PBS	23.6	Yes	n. r.	166 ± 19	Yes/Yes
PBS/20%CaDMP	27.3	Yes	V-2	6 ± 3	Yes/Yes
PBS/20%ZnDMP	25.1	Yes	V-2	11 ± 6	Yes/Yes
PBS/20%AlDMP	23.6	No	V-2	17 ± 5	No/Yes

[a] A standard deviation for all presented LOI values is ±0.2 vol%. [b] t_1+t_2 – average total afterflame time, t_1 and t_2 refer to the flaming combustion time after the removal of the first flame and the second flame, respectively.

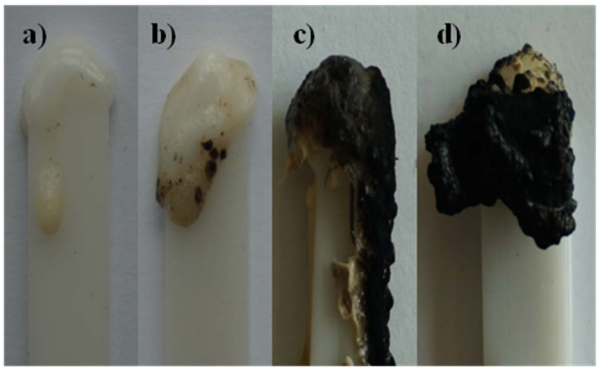

Fig. 1 Digital images of the specimens after LOI test recorded for: (a) neat PBS, (b) PBS/20%CaDMP, (c) PBS/20%ZnDMP, and (d) PBS/20% AlDMP.

extrusion, injection moulding *etc.*[16] In all of these industrial processes the viscoelastic melt flow proceeds at relatively high shear rates that can reach the level of *ca.* 10^5 s^{-1}.[17,18] In contrast, the dripping and melt flow occurring during several small-scale fire tests (*e.g.*, UL-94 and LOI), is associated with much lower shear rates.[19–21] Therefore for all the studied materials, we have decided to carry out rheological measurements in oscillatory mode and a wide range of the angular frequencies (0.1–628 rad s^{-1}). Fig. 2 shows the complex viscosity $|\eta^*|$, loss factor (tan δ), storage modulus (G') and loss modulus (G″) as a function of angular frequency (ω) at 190 °C.

All $\log|\eta^*|$ *versus* $\log\omega$ curves presented in Fig. 2a show shear thinning effect typical for polymer melts, which is the most pronounced for PBS/20%AlDMP. The viscosity curves of neat PBS and of PBS/20%ZnDMP have a very similar profile and are characterized by a Newtonian plateau at low frequencies (*i.e.*, for ω between 0.1 and 0.6 rad s^{-1}). On the contrary, the analogous curves recorded for the AlDMP- and CaDMP-containing composites show continuous increase in $|\eta^*|$ towards lower frequencies.

It should be noted that over the applied frequency range PBS/20%AlDMP is characterized by the highest $|\eta^*|$ among all the investigated composites and neat PBS. In addition, the differences between the value of $|\eta^*|$ and the values of this parameter for other materials increase following a decrease in the angular frequency. Moreover, in the low-frequency region, the incorporation of AlDMP particles leads to a four-order-of-magnitude increase in $|\eta^*|$ values (at $\omega = 0.1$ rad s^{-1} a difference between $|\eta^*|$ of PBS/20%AlDMP and a neat PBS reaches 1.95×10^4 Pa s). At the same time, the presence of CaDMP and ZnDMP has a plasticising effect and the $|\eta^*|$ is decreased by approximately 210 Pa s at $\omega = 0.1$ rad s^{-1} compared to neat PBS. In case of the high frequency region (*i.e.*, for ω above 6 rad s^{-1}), a decrease in the difference between the $|\eta^*|$ of the composites and $|\eta^*|$ of the unmodified polymer can be observed – and this trend strengthens with an increase in frequency, in particular for ZnDMP, which almost completely loses its plasticising effect on PBS (at $\omega = 628$ rad s^{-1} PBS/20%ZnDMP exhibits $|\eta^*|$ *ca.* 2.5% lower than neat PBS).

The differences in the rheological behaviour of PBS/20% AlDMP and PBS/20%CaDMP in comparison to neat PBS and PBS/20%ZnDMP are also distinct when the changes in G' over the angular frequency are analysed. As we can see in Fig. 2c, the slope of $\log G' = f(\log\omega)$ is less than any of corresponding curves for the two former composites in the low frequency region. In particular, for PBS/20%AlDMP composite the $\log G' = f(\log\omega)$ and $\log G'' = f(\log\omega)$ curves start to develop a plateau at low angular frequencies. This developing plateau is an indicator of the existence of an apparent yield stress for PBS/20%AlDMP melt.[22–24]

Due to the distinct qualitative characteristics of the $\log|\eta^*| = f(\omega)$ curves, the investigated materials can be categorized into two groups: (1) materials exhibiting Newtonian plateau at low frequencies: neat PBS, PBS/20%ZnDMP (2) materials without Newtonian plateau at low frequencies showing an increase in $|\eta^*|$ with decreasing ω: PBS/20%AlDMP, PBS/20%CaDMP. The occurrence of an increase in $|\eta^*|$ following a decrease in ω, just as in the case of PBS/20%AlDMP and by PBS/20%CaDMP as well as an apparent yield stress (exhibited by PBS/20%AlDMP) have been already reported for thermoplastic melts containing anisotropic fillers such as clay or expanded graphite in PBS,[25,26] multiwalled carbon nanotubes in polycarbonate,[24] carbon fibers or mica in polyethylene,[27,28] as well as talc in iPP.[29] According to the literature data, the increase in $|\eta^*|$ in the low-frequency region and the occurrence of apparent yield stress can be attributed to the complex filler–filler interactions resulting in the formation of an interconnected filler structures.[22,24,25,27] Thus, a different rheological behaviour exhibited by PBS/20% MtDOP composites in the low-frequency region can occur as

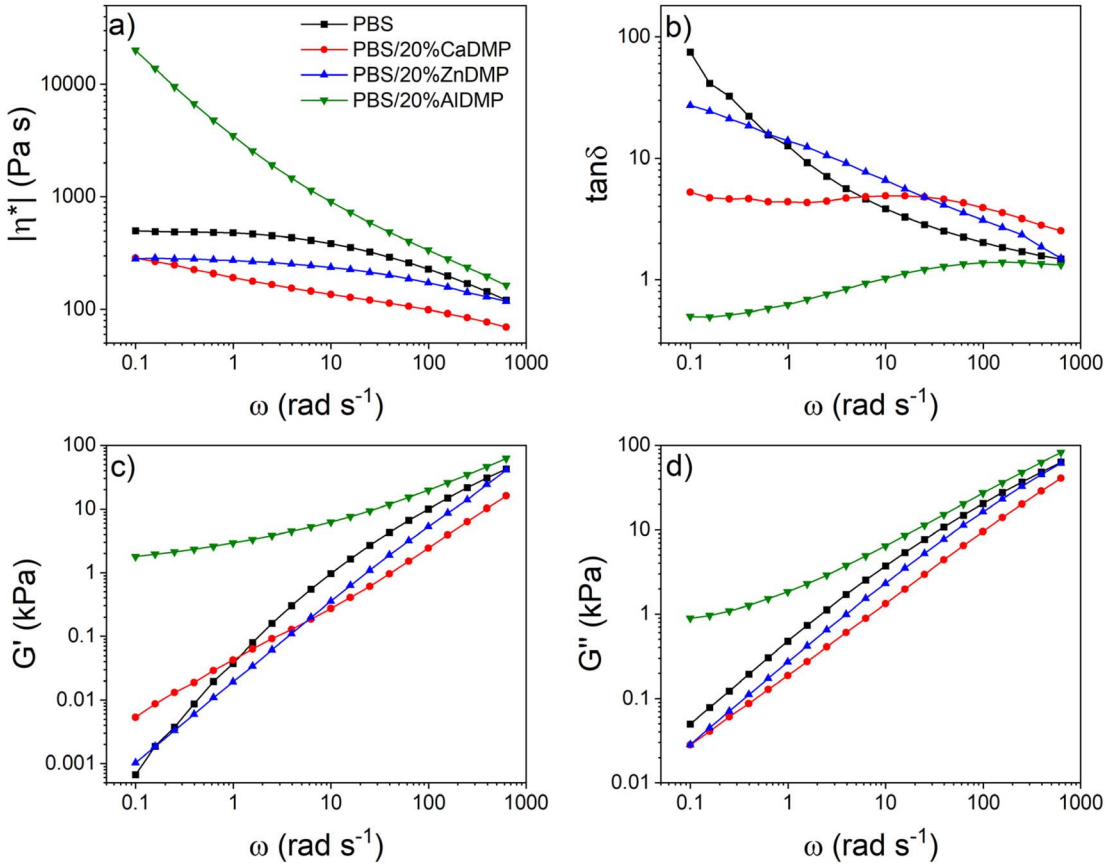

Fig. 2 Angular frequency dependency of (a) complex viscosity, (b) loss factor, (c) storage modulus, and (d) loss modulus recorded at 190 °C for PBS and its composites with 20 wt% of MtDOPs.

a consequence of the differences in morphology of the respective fillers, which form highly anisotropic 1D particles (AlDMP and CaDMP) or spherical-like domains (ZnDMP) (see Fig. S1 in SI). Moreover, at 190 °C ZnDMP exists in its composite with PBS as a viscous liquid having small ability to build a highly agglomerated/percolated 3D structures, whereas AlDMP or CaDMP particles do not melt, retain their anisotropic shape and at low frequencies can freely interact with each other forming a 3D interparticle network less prone to flow. However, the contribution of the strengthened polymer–filler interactions between PBS and AlDMP to the observed increase in $|\eta^*|$, G' and G'' cannot be excluded, especially that in the high-frequency region values of these 3 parameters determined for PBS/20% AlDMP are higher compared to the characteristics of neat PBS. By analogy, the lower values of $|\eta^*|$, G' and G'' for PBS/20% CaDMP and PBS/20%ZnDMP than neat PBS in high-frequency region could be indicative of weak PBS_{liquid} – $CaDMP_{solid}$ and PBS_{liquid} – $ZnDMP_{liquid}$ interactions.

It is worth noting that for neat PBS and its composites with CaDMP or ZnDMP in the entire frequency range G'' exceeds G' (*i.e.*, $\tan\delta > 1$, Fig. 2b) indicating the liquid-like viscoelastic behaviour of these systems. However, for neat PBS and PBS/20% ZnDMP the viscous properties decreases monotonically with increasing angular frequency from 0.1 to 628 rad s^{-1}, whereas for PBS/20%CaDMP one can also observe an additional effect of $\tan\delta$ value increase at ω between 2.5 and 25 rad s^{-1}.

The only material in the tests in which the elastic properties prevail over the viscous ones was PBS/20%AlDMP, albeit this occurred only in the low-frequency region (*i.e.*, $G' > G''$ and $\tan\delta < 1$) – at the frequency of 8.75 rad s^{-1} a crossover point appears ($G' = G''$, $\tan\delta = 1$) giving the relaxation time of 0.715 s. Above that point the viscoelastic response of PBS/20%AlDMP becomes predominantly viscous. It should be noted that the existence of a well-developed AlDMP interparticle network within molten PBS can account for the predominantly elastic behaviour of PBS/20%AlDMP in the low-angular frequency region, while its destruction at higher frequencies increases liquid-like properties.

We recorded $|\eta^*|$ *versus* ω plots at the temperatures from 170 to 210 °C to gain more insight into the rheological properties of PBS/20%MtDOPs composites (Fig. S2 in SI). While for neat PBS and PBS/20%ZnDMP composite $|\eta^*|$ decreases with increasing temperature in entire range of angular frequency, in the case of the other two studied materials such phenomenon occurs only above a certain threshold of ω (62.8 rad s^{-1} for PBS/20%AlDMP and 3.96 rad s^{-1} for PBS/20%CaDMP) and a positive viscosity-temperature dependence is exhibited at the low-frequency region. Although the $|\eta^*|$ *versus* ω curves of PBS/20%AlDMP or PBS/20%CaDMP recorded at different temperatures do not

intersect (crossover) at a single point, it is possible to distinguish the frequency region where the transition between the positive and negative dependence of $|\eta^*|$ on temperature takes place – for PBS/20%CaDMP it is located between 0.16 and 3.96 rad s^{-1}, whereas for PBS/20%AlDMP between 3.96 and 99.5 rad s^{-1}. It is also worth noting that for CaDMP-containing composite the effect of increasing of $|\eta^*|$ towards lower ω within the low-frequency regime becomes increasingly significant at higher temperatures.

An increase of $|\eta^*|$ in the low angular frequency region with rising temperature has been already reported for polylactide–graphene, poly(ethylene oxide)-clay and polyurethane–carbon nanotubes composites. In addition, this phenomenon was accompanied by increasing elastic response with an increase of temperature.[30–32] In order to examine the effect of temperature on the solid-like behaviour of PBS and its composites with MtDOPs, the data obtained in oscillatory rheometry are compiled in the form of Van Gurp–Palmen plots (Fig. S3 in SI). As can be seen in Fig. S3a and c the loss angel (δ) values at low complex modulus (G^*) (*i.e.* at low ω) for PBS and PBS/20% ZnDMP tend towards 90° regardless of the temperature. This indicates that PBS and PBS/20%ZnDMP melts behave mostly liquid-like in the low angular frequency region and temperature has no influence of their elastic response. In opposite, for composites containing CaDMP and AlDMP Van Gurp–Palmen plots deviate from 90° at low G^* and this deviation is more visible as the temperature rises. It should therefore be concluded, that an increase of the temperature promote the solid-like behaviour of PBS/20%CaDMP and PBS/20%AlDMP melts in the low frequency region. Thus, in the CaDMP- and AlDMP-containing systems positive complex viscosity-temperature dependence at low ω goes hand in hand with an increase in elastic response. Similar to Yu *et al.*, we attribute this anomalous rheological behaviour with a combination of strengthened filler–filler and polymer–filler interactions at higher temperatures.[32] We assume that the reason for the former can be attributed to an increased mobility of CaDMP- and AlDMP rod-like particles at higher temperatures and thus an increased ability to form a interparticle network. On the other hand enhanced polymer–filler interactions could be associated with more intense occlusion of polymer segments in the interparticle voids of the AlDMP and CaDMP 3D networks at higher temperatures.

The dripping behaviour of PBS/20%MtDOP materials observed during the LOI and UL-94 tests can be explained by the evaluation of their rheological properties estimated in the low angular frequency region. Among the investigated MtDOPs only AlDMP successfully prevent melt flow and dripping of the samples subjected to LOI and UL-94 tests. This is due to a much stronger increase in $|\eta^*|$ (Fig. 2a) and complex modulus (G^*) (Fig. S4 in SI) caused by AlDMP, when compared with the other two MtDOPs. G^* forms a quantitative measure of the resistance to the deformation and the shape of the $\log G^* = f(\log \omega)$ curve indicates the existence of a relative high apparent yield strength for PBS/20%AlDMP composite. This leads to a conclusion that the effect of the gravitational force acting on the PBS/20% AlDMP samples during both self-extinguishing tests is not sufficiently high to create the stress needed to induce the viscoelastic melt flow. In contrast, the presence of CaDMP or ZnDMP seems to promote melt flow of PBS matrix since at the low-frequency region their composites exhibit $|\eta^*|$ and G^* that are lower than the corresponding values of neat PBS (Fig. 2a and S3 in SI).

3.3 Mass loss calorimetry test

The MLC was used to investigate the forced combustion of PBS and its composites filled with 20 wt% of MtDOPs. The external heat flux 50 kW m^{-2} was selected to simulate the developing fire scenario.[33] The results of the MLC test are presented in two ways: graphically as the heat release rate (HRR) and mass loss rate (dm/dt) over the time curves (Fig. 3) and quantitatively (Table 2) as the numerical values of primary physicochemical parameters of combustion such as: time to ignition (TTI), pHRR, time to peak of heat release rate (TTpHRR), fire growth rate (FIGRA), THE, avEHC and CY.

PBS composites with 20 wt% of MtDOPs are easier to ignite than neat PBS as evidenced by a shortening of TTI by 4, 10 or 12 s for AlDMP-, ZnDMP- or CaDMP-containing materials, respectively. After ignition PBS burned rapidly reaching pHRR

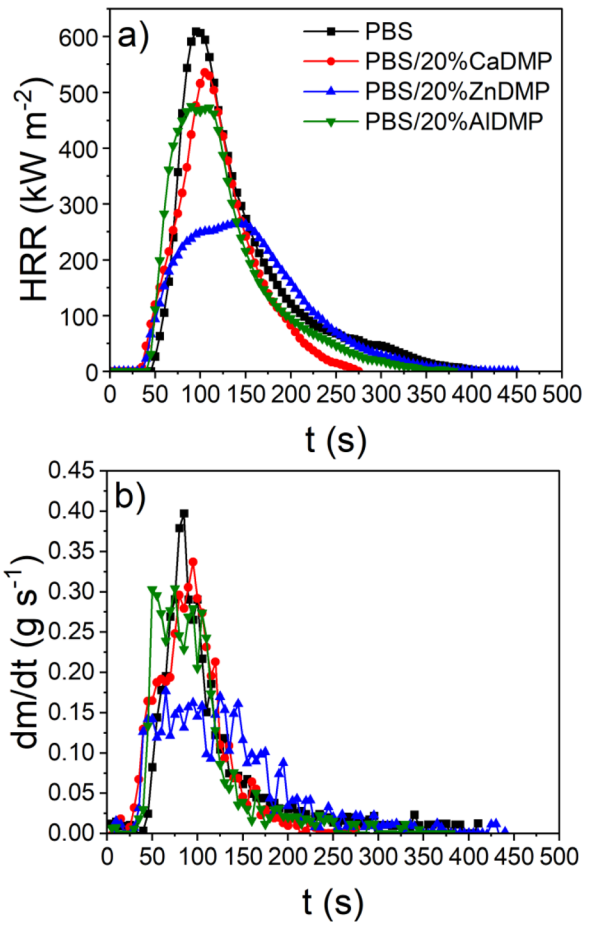

Fig. 3 The results of MLC tests carried out for PBS and its composites containing 20 wt% of MtDOPs: (a) heat release rate, and (b) mass loss rate curves.

Table 2 Combustion parameters estimated by means of the MLC test

Material	TTI (s)	pHRR (kW m^{-2})	TTpHRR (s)	FIGRA (kW m^{-2} s^{-1})	THE (MJ m^{-2})	avEHC (MJ kg^{-1})	CY (wt%)
Neat PBS	43 ± 2	611 ± 8	100 ± 5	6.35 ± 0.20	55.24 ± 2.72	20.44 ± 0.50	4.53 ± 2.17
PBS/20%CaDMP	31 ± 3	536 ± 14	98 ± 8	5.56 ± 0.49	46.44 ± 1.63	17.69 ± 1.08	10.96 ± 1.19
PBS/20%ZnDMP	33 ± 2	264 ± 5	130 ± 18	2.82 ± 0.17	41.72 ± 1.99	16.50 ± 0.56	16.72 ± 0.63
PBS/20%AlDMP	39 ± 3	483 ± 16	98 ± 8	5.84 ± 0.11	49.52 ± 1.42	18.58 ± 0.60	9.57 ± 0.82

of 611 kW m^{-2} after 100 s from the start of the MLC test. An introduction of 20 wt% of CaDMP, ZnDMP or AlDMP to PBS matrix decreased pHRR by 12%, 57% and 21% respectively. At the same time, the TTpHRR parameter was practically unaffected for PBS/20%CaDMP and PBS/20%AlDMP and increased by 30 s for PBS/20%ZnDMP, compared to neat PBS. Among the investigated materials, some differences in the shape of the HRR over the time curves can be observed (Fig. 3a): in the case of neat PBS and its composite with CaDMP a sharp peak is clearly detected. On the contrary, profiles obtained for PBS/20% AlDMP and PBS/20%ZnDMP are characterized by a small (*i.e.*, 30 and 80 s wide, respectively) plateau located near pHRR and indicative of a semi-steady burning behavior. Concurrently, FIGRA is also positively affected by MtDOPs as its values estimated for all the studied composites decrease. Hence, this indicates a lower tendency to spread fire compared to the neat polymer. The lowest FIGRA is observed in the case of PBS/20% ZnDMP (FIGRA decreased by 56%), while for PBS/20%AlDMP only the 8% reduction of FIGRA is detected.

Fig. 3b shows that the incorporation of MtDOPs into PBS results in a slower emission of the volatiles and increased CY (Table 2). Furthermore, the combustion of PBS/20%MtDOPs volatile products was less exothermic in comparison with a combustion of these evolved by a neat PBS (reduction of the heat available per unit of mass loss – avEHC). Both these phenomena lead to a decrease of THE of MtDOPs-containing composites regarding this parameter obtained for neat PBS. A simultaneous increase in the amount of solid residue left after combustion (neat PBS < PBS/20%AlDMP < PBS/20%CaDMP < PBS/20%ZnDMP) and decrease of the avEHC value (PBS > PBS/20%AlDMP > PBS/20%CaDMP > PBS/20%ZnDMP) indicate a dual (*i.e.*, occurring in both the condensed and gas phase) flame retardancy mode of action of the studied MtDOPs.

3.4 Char residue characterization

With the purpose of further investigation into how MtDOPs act as flame retarders of PBS, the morphology and chemical composition of char residues resulting from combustion in the MLC apparatus were characterised *via* digital photos, SEM, EDS, FTIR and Raman spectroscopy.

After the ignition of PBS/20%ZnDMP, the sample expanded gradually increasing its thickness from 2.1 mm to approximately 20 mm at the highest point (see Fig. S5 in SI). This is in good conformity with the foaming of PBS/20%ZnDMP observed during LOI test. On the other hand the samples of neat PBS, as well as its composites with CaDMP or AlDMP did not substantially change their volume during combustion.

The optical images show that the solid residue after combustion of PBS/20%AlDMP (Fig. S6c in SI) has some cracks, while those formed by the CaDMP- and ZnDMP-containing materials exhibits continuous surface (Fig. S6a and b). The thickest char residue forms PBS/20%ZnDMP, even though its foamed structure settled in the final combustion phase and it exhibits the most compact structure. SEM micrographs presented in Fig. 4 provide more insight into an internal structure of the obtained solid residues. The char residue from PBS/20% AlDMP consists of loosely bound rod-like particles that exhibit 1D morphological features similar to those of neat AlDMP. The

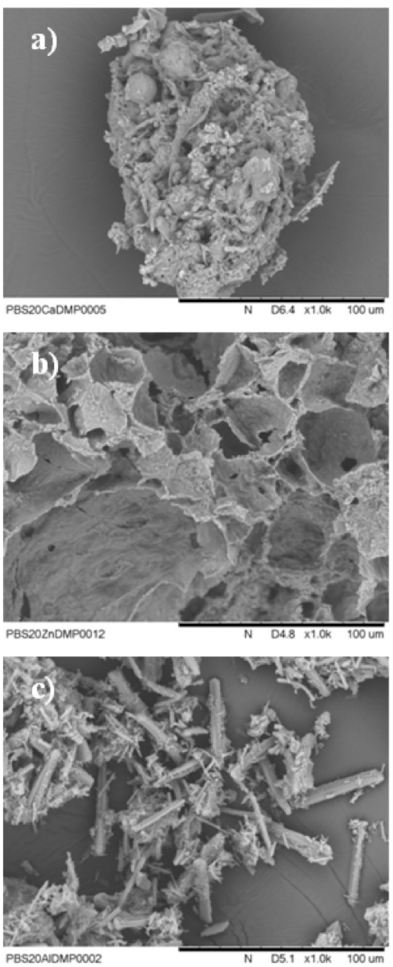

Fig. 4 SEM images of internal structures of the solid residues obtained after the MLC combustion of the PBS composites containing 20 wt% of: (a) CaDMP, (b) ZnDMP and (c) AlDMP. All images recorded at a magnification of 1000×.

same phenomenon was recorded in the case of solid thermolysis product of neat AlDMP.[15] Solid residue derived from PBS/20%CaDMP is characterized by a more compact and complex structure, which significantly differs from that of the particles of neat filler – Fig. 4a and S7 (SI) demonstrate the existence of spherical-like particles of various sizes. Finally, SEM image of the solid residue derived from the ZnDMP-containing composite confirms its foamed structure since one can observe hollow, rounded domains with sizes ranging from *ca.* 5 to 110 μm (Fig. 4b).

We have characterized neat MtDOP fillers and the char residues from combustion of their PBS composites in terms of the phosphorus to metal (P/Mt) molar ratio – the results of elemental analysis by means of EDS technique are presented in Table 3. Those data indicate a high agreement between the P/Mt molar ratio estimated from EDS measurements and the values predicted for neat fillers on the basis of their stoichiometry (*i.e.*, 2.00 for CaDMP and ZnDMP, or 3.00 for AlDMP). As a result of the combustion of PBS/20%MtDOPs, the P/Mt molar ratio decreases significantly indicating emission of the phosphorus-containing species into a gas phase – such emissions have been already proved experimentally by detection of TMP in the condensate obtained during pyrolysis of pristine CaDMP, ZnDMP or AlDMP.[9] One can expect that emission of the phosphorus-containing species into a gas phase during combustion of PBS/20%MtDOP composites might play a key role in the already mentioned decrease of avEHC.

In order to gain more insight into chemical composition of char residues from PBS/20%MtDOPs combustion, their FTIR analysis was performed. All recorded spectra presented in Fig. 5 demonstrate medium to very strong absorption bands within the 680–800, 900–1000, and 1100–1300 cm^{-1} spectral regions. These could be linked to the respective symmetric and antisymmetric stretching vibrations within the bridging P–O–P group, as well as antisymmetric stretching mode of the "external" (non-bridging) P–O bond ($P–O_{ext}$). Therefore, during the combustion of PBS/20%MtDOP composites a transformation of MtDOPs into condensed phosphates can be postulated.[34–36] These findings are also supported by the results of EDS characterization, since the P/Mt values estimated for the PBS/20%MtDOP combustion char residues (see Table 3) are in-between theoretical values calculated for di- or trivalent metal: pyrophosphates (1 or 1.5, respectively) and metaphosphates (2 or 3, respectively). Therefore, it can be forecasted that a mixture

Table 3 Phosphorus to metal (P/Mt) molar ratio estimated by means of EDS for raw MtDOPs and the solid residues obtained during combustion of PBS/20%MtDOP composites

	P/Mt (mol mol^{-1})	
MtDOP	Neat MtDOP	Char residue from PBS/20%MtDOP combustion
CaDMP	1.89 ± 0.26	1.31 ± 0.06
ZnDMP	1.99 ± 0.18	1.60 ± 0.15
AlDMP	3.02 ± 0.21	1.94 ± 0.03

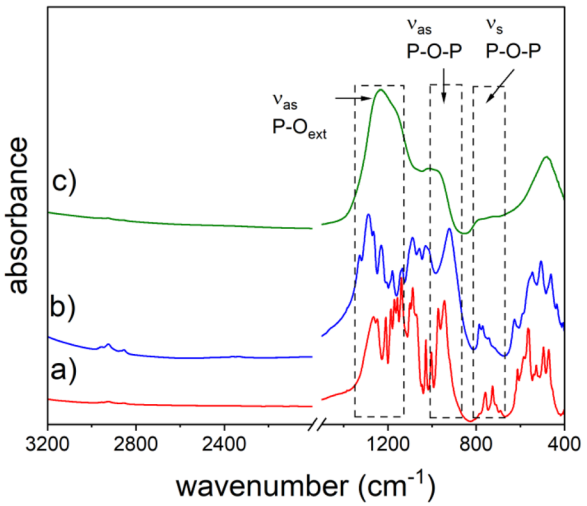

Fig. 5 FTIR spectra of the solid residues obtained during MLC combustion of the PBS composites containing 20 wt% of: (a) CaDMP, (b) ZnDMP and (c) AlDMP.

of these two groups of inorganic phosphates form the analysed residues, although the possibility of presence of higher homologues of metal pyrophosphates (*i.e.*, derivatives with a condensation degree exceeding 2) or metal ultraphosphates cannot be entirely dismissed. Indeed, in the case of PBS/20% ZnDMP char residue the presence of a certain fraction of zinc ultraphosphates can be deduced from the additional absorption band located at 1327 cm^{-1} and ascribed to antisymmetric stretches of non-bridging P–O bonds in ultraphosphate moiety.[34]

The Raman spectra of the solid residues from the combustion of PBS/20%MOPs composites (Fig. 6) contain two high-intensity signals centred at 1594 and 1321 cm^{-1}. The former is assigned to the $C_{sp^2}–C_{sp^2}$ in-plane stretching in a highly

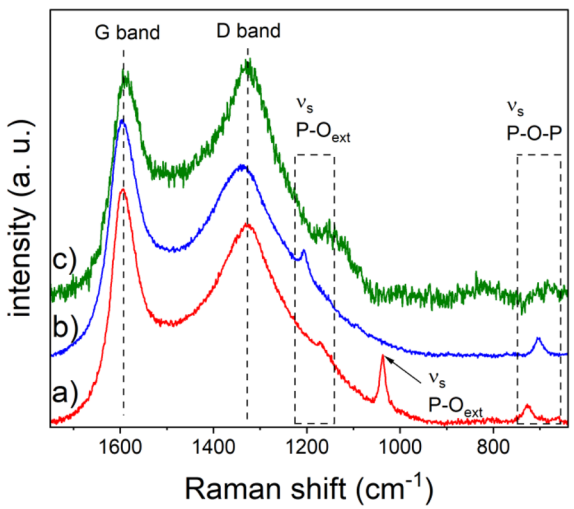

Fig. 6 Raman spectra of the solid residues obtained during MLC combustion of the PBS composites containing 20 wt% of: (a) CaDMP, (b) ZnDMP and (c) AlDMP.

ordered graphene or graphite (G band), whereas the latter arises from the vibrations of disordered sp^3 carbon (D band).[37–40] This observation indicates that PBS macromolecules and/or MtDOPs undergo partially carbonization during combustion of PBS/20% MtDOPs composites. Moreover, Raman spectra also support the prior conclusion regarding the formation of the condensed phosphates of calcium, zinc or aluminium during combustion of PBS/20%MtDOPs materials. They demonstrate some weak absorption bands located in the spectral regions 1205–1150 cm^{-1} and 750–650 cm^{-1} related to $\nu_s(P–O_{ext})$ and $\nu_s(P–O–P)$ vibrations in condensed-phosphates, respectively. Interestingly, the Raman spectrum of the Ca-containing solid residue is distinguished by an additional peak at 1037 cm^{-1}, which can be ascribed to $\nu_s(P–O_{ext})$ mode within PO_3 groups of pyrophosphates (Fig. 6a).[34,41]

3.5 Flame – retardant mode of action

In general, the effect of flame retarders on the flammability of polymers during the cone calorimeter test is often discussed in terms of three main modes of action: charring (Ch), effect of barrier protective layer – both in condensed phase (BaPL) and flame inhibition (FI) in the gas phase. These three modes of action were quantified for the currently studied MtDOP-containing PBS composites according to eqn (S1)–(S3) (SI)[42,43] and the results of such calculations are summarized in Table 4. As can be seen in Table 4, the charring effect in PBS/20% MtDOPs composites increases in the order PBS/20%AlDMP < PBS/20%CaDMP < PBS/20%ZnDMP, *i.e.* in the same order in which the CY increased during TGA under N_2 for raw MtDOPs.[9] As indicated by FTIR and Raman spectra, the solid residues from combustion of PBS/20%MtDOP composites contain condensed phosphates of the respective metal along with some carbonaceous deposit of mixed ordered–disordered nature. Thus, the calculated charring effect can be associated with dilution of the practically non-charring polymer matrix with partially-charring filler's particles, leading to a lower fuel emission into the gas phase.

As could be expected, the barrier and protective properties of the Zn-containing char are the best among the investigated PBS composites. Substantially high value of BaPL (42.8%) for PBS/20%ZnDMP indicates, that the coherent, intumescent char forming during combustion of this material serves as efficient barrier for heat and mass transfer between condensed and gas phase. Hence, pyrolysis of the deeper layers of polymer and the rate of the combustible volatiles release are effectively slowed down (Fig. 3b). In addition, HRR for this composite was extremely decreased compared to neat PBS (Fig. 3a).

Table 4 Assessment of the main flame-retardant modes of action exhibited by PBS composites filled with 20 wt% of MtDOP

Composite	Ch (%)	BaPL (%)	FI (%)
PBS/20%CaDMP	6.7	−4.3	13.5
PBS/20%ZnDMP	12.8	42.8	19.3
PBS/20%AlDMP	5.3	11.8	9.1

The poor barrier properties of the Ca- and Al-containing chars can be attributed to their structure consisting of spherical-like or loosely bound rod-like particles coupled with an absence of a highly compact structure (Fig. 4a and c). As a consequence, the BaPL parameter is for PBS/20%CaDMP or PBS/20%AlDMP composites much lower, when compared with BaPL obtained for foamed PBS/20%ZnDMP.

The highest flame inhibition effect is demonstrated after the incorporation of ZnDMP into the PBS matrix, while CaDMP and AlDMP are less active flame retardants in the gas phase (Table 4). Several scientific groups have already indicated that many phosphorous-containing compounds, including phosphoric acid esters, decompose in the flame to the oxophosphorus moieties such as PO, HPO, HOPO, $HOPO_2$, or PO_2. These species easily react with $[OH]^{\bullet}$ and $[H]^{\bullet}$ radicals and reduce the exothermic effect of the reactions taking place in the gas phase.[44–47] This knowledge, along with the previously discussed differences in the P/Mt molar ratio between raw MtDOPs and the solid residues resulting from combustion of their PBS composites (Table 3), led us to undertake evolved gas analysis (EGA) using the TGA–FTIR technique.

As can be seen from the data presented in Table S1 and Fig. S8–S11 (SI), under inert gas conditions neat PBS has the highest thermal stability and decomposes between *ca.* 369 and 457 °C. In the case of the PBS/20%MtDOPs composites, the incorporation of MtDOPs into the PBS matrix substantially decreases all the characteristic temperatures of pyrolysis and changes its nature from a single-step (for the unmodified PBS) into a two-step process (for the AlDMP- and ZnDMP-containing systems), or multistep transformation (for PBS/20%CaDMP). Among the investigated composites, the system containing CaDMP particles is the most susceptible to thermolysis (its $T_{98\%}$ value is approximately 316 °C and is about 53 °C lower than that of neat PBS), whereas PBS/20%AlDMP exhibits the highest $T_{98\%}$ value (approximately 340 °C) and its sample reaches mass stabilization most rapidly after the completion of the degradation process (the difference between its $T_{98\%}$ and T_{end} values is only *ca.* 54 °C). It is noteworthy that pyrolytic degradation of PBS/20%ZnDMP proceeds within the largest temperature range (its T_{end}–$T_{98\%}$ value equals *ca.* 116 °C) and ends approximately 22 °C lower than in the case of neat polymer matrix.

The results of EGA (Fig. S9c, S10c and S11c in SI) clearly indicate the presence of TMP molecules among the volatile products of thermal degradation of the investigated composite systems, regardless of the type of the applied filler. Interestingly, at the early stage of this process (when the weight loss does not exceeds *ca.* 10 wt%) the recorded FTIR spectra are practically identical with that of the reference TMP sample (see Fig. S13), showing its characteristic absorption bands located around 2963 cm^{-1} (C–H stretching), 1302 cm^{-1} (P═O stretching), 1056 cm^{-1} (P–O–C anti-phase stretching) and 847 cm^{-1} (P–O–C in-phase stretching).[48] Interestingly, another feature that distinguishes PBS/20%ZnDMP from other two composites is a relatively low concentration of TMP molecules released into the gas phase, as indicated by an increased noise-to-signal ratio and less well-defined TMP-related FTIR absorption bands. This observation suggests lower emissions of phosphorus-

containing compounds into gaseous phase during thermal degradation of this material. This finding is also consistent with the average phosphorus weight concentration in the volatiles estimated from the previously mentioned EDS analysis (eqn (S11) and S14 in SI). The average phosphorus weight concentration in the volatiles during combustion in MLC is for PBS/20%ZnDMP the lowest among PBS/20%MtDOPs composites.

Upon further heating, the main weight loss step occurs and EGA reveals the appearance of FTIR absorption bands that can be attributed to the typical volatile products formed during PBS decomposition, *i.e.*, succinic anhydride (1811 cm^{-1}, C=O stretching) and tetrahydrofuran (2981 cm^{-1}, C–H stretching; 920 cm^{-1}, CH_2 twisting).[49,50] We should note that although the time/temperature profiles recorded for the FTIR diagnostic bands of TMP (see Fig. S12 in SI) suggest that the latter is also released at this stage of thermal degradation of the composites, this statement is not justified due to the partial overlapping of adjacent absorption bands related to products of PBS decomposition. These bands contribute to the "non-zero" FTIR absorption at 847 cm^{-1} and 1302 cm^{-1} even in the case of neat PBS. Similar phenomena (*i.e.*, the overlapping of TMP-related absorption bands) may explain the apparent detection of THF traces at the initial stage of thermal degradation of the investigated composites and the presence of the low-absorbance peaks for 920 cm^{-1} and 2982 cm^{-1} FTIR band profiles within the 30–35 minutes range.

It is worth noting that avEHC of PBS/20%MtDOP composites is not a monotonic decreasing function of average phosphorus weight concentration in the volatiles. A similar minimum of avEHC on the phosphorus concentration in the gas phase was observed by Rabe *et al.* in epoxy resin doped with red phosphorus as flame retardant. Based on own investigations and findings of another researchers[51–53] Rabe and co-authors have devised a model avEHC = *f*(phosphorus-concentration in gas phase) curve where avEHC initially declines as the phosphorus-amount in the gas phase rises, but beyond a specific phosphorus concentration, avEHC begins to increase with a higher phosphorus-concentration. Authors suggest that an increase in avEHC with higher amounts of phosphorus in the gas phase is due to the burning of phosphorus-containing species. This could be the reason why PBS/20%ZnDMP exhibited the lowest and PBS/20%AlDMP the highest avEHC in the MLC test.

Another aspect is related to the assumption on the boosting effect of the intumescent Zn-containing char on the flame inhibition by phosphorous-containing species.[9] Korobeinichev *et al.* postulated that an excess of the fuel leads to reduction of the flame inhibition effectiveness of TMP in the $CH_4/O_2/Ar$ flame – based on detection of CH_3PO_2 in the fuel rich flames the authors suggested, that this chemical moiety and some other products of an incomplete combustion of TMP are not able to recombine $[H]^{\bullet}$ and $[OH]^{\bullet}$ radicals in the flame.[54] As already discussed, due to the barrier properties of the formed intumescent char, the presence of ZnDMP effectively reduces the release rate of the volatiles and one could expect that the flame during PBS/20%ZnDMP combustion should be leaner in fuel (thus having lower concentration of inactive phosphorus-containing species) than the flames produced by the other two composites. However, this is only a hypothesis that needs further experimental verification.

Finally, the flame retardant mechanism of MtDOPs with regard to the self-extinguishing properties of their PBS composites analysed during the LOI test should also be addressed. Similar to their iPP-based analogues, the LOI values estimated for PBS/20%MtDOP composites do not correlate with the primary physicochemical parameters of combustion determined in the MLC test. The lack of such correlation is a well-known fact that has been widely reported in the literature.[55–57] The main reasons for this include: (1) prevention of melt flow and dripping phenomena in the case of measurements carried out by cone calorimeter, (2) differences in the mode of exposition of the sample to the external heat flux which is permanent during combustion in the cone calorimeter and temporary during the LOI test.

Easy dripping and flow often increases the LOI values *via* the mass and heat transfer from the combustion zone to the lower part of the sample.[46,55,58] As shown by the rheological tests mentioned above, the incorporation of CaDMP or ZnDMP into PBS results in lower $|\eta^*|$ and G^* (Fig. 2a and S4 in SI) values in the low frequency region than those of neat PBS and do not prevent dripping and melt flow during LOI test. It can been therefore assumed, that the improvement of melt flow by these two fillers contributes to the better behaviour of their PBS composites subjected to LOI tests. In contrast, the incorporation of 20 wt% of AlDMP into PBS leads to a substantial increase in $|\eta^*|$ and G^* at low frequencies and consequently suppress dripping and melt flow.

Naturally, less energetic combustion can also positively influence LOI.[59] However, for the purpose of our consideration concerning PBS/20%MtDOP composites it is not correct to directly correlate THE or avEHC estimated during the MLC test with the results of LOI: in MLC the applied constant external heat flux of 50 kW m^{-2} is related to the developing fire scenario, while during LOI test the burning part of sample is subjected only to the internal heat flux resulting from its own flame (excluding the ignition stage). A much more feasible approach would related to developing a correlation between the LOI values and THE or avEHC at significantly lower irradiations or even with the THE or avEHC values extrapolated to the 0 kW m^{-2} irradiance. This is due to a well-established fact that TTI, pHRR, THE or avEHC are dependent on the applied irradiation.[60,61] In the light of the above arguments, it is not surprising that PBS/20%CaDMP, although showing inferior fire behavior in the MLC test when compared to PBS/20%ZnDMP, exhibits a higher LOI value (27.3 vol%) compared to the latter system (25.1 vol.). From our viewpoint the improvement of LOI due to the presence of CaDMP or ZnDMP particles can be related both to melt flow/dripping effect and less energetic combustion compared to neat PBS, although the quantification of the contribution of each of these two phenomena on the basis of the results obtained in this work is not possible. In the case of AlDMP, the negative contribution related to melt flow and dripping suppression seems to be of the same level as positive effect of the decreased THE resulting in no differences between LOI values for PBS/20%AlDMP and neat PBS. To conclude,

results of the MLC test simulate the fire behaviour of PBS and its composites with MtDOPs in a developing fire scenario, while the data obtained by means of LOI and UL-94 methods are related to the self-extinguishing properties of the investigated materials.

4 Conclusions

In this paper, the effect of incorporation of 20 wt% of CaDMP, ZnDMP or AlDMP on flame retardancy and rheological properties of PBS is investigated and discussed in detail for the first time.

With addition of MtDOPs to PBS matrix the reaction to small fire was improved, thus, all composites are rated as V-2 and LOI increased from 23.6 vol% for neat PBS to 25.1 vol% and 27.3 vol% for PBS/20%ZnDMP and PBS/20%CaDMP respectively. AlDMP-containing composite, opposite to its iPP-based analogues, show unaffected LOI value with respect to the pristine PBS, which is most probably related to the melt and dripping suppressing by AlDMP *via* a rheological effect. Regarding the rheological properties of PBS and PBS/20%MtDOPs melts, CaDMP and ZnDMP show a plasticising effect reducing the $|\eta^*|$, G' and G'', while PBS/20%AlDMP exhibit much higher values of $|\eta^*|$, G' and G'', especially at the low frequencies including the occurrence of apparent yield stress, compared with a pristine PBS. Moreover CaDMP- and AlDMP-containing composites show in low frequency region a unusually positive viscosity-temperature dependence.

In MLC test simulating a developing fire scenario all examined MtDOPs caused reduction in pHRR, THE, avEHC and FIGRA. The best enhancement is brought by ZnDMP, as it lowers pHRR by 57%, THE by 24%, avEHC by 19% and FIGRA by 56%. Based on results of MLC, SEM, EDS, FTIR, Raman spectroscopy, as well as TGA–FTIR the possible flame retardancy mechanism of MtDOPs in PBS was proposed. It considered dual acting of MtDOPs in the gas phase (reduction in avEHC) due to liberating of TMP during their thermall decomposition and in the condensed phase. The latter effect was associated with the production of a solid residue consisting of a mixture of condensed metal phosphates and elemental carbon. In addition, the best fire-retardant properties of ZnDMP were related to its potential for the formation of a barrier and protective intumescent char.

Author contributions

Mateusz Kullas: conceptualization, investigation, methodology, formal analysis, data curation, writing – original draft. Maciej Dębowski: resources, funding acquisition, formal analysis, writing – review & editing, supervision. Paweł Groch: investigation, methodology, formal analysis, writing – review & editing. Anna Czajka-Warowna: investigation, methodology. Krystyna Czaja: conceptualization, writing – review & editing, supervision.

Conflicts of interest

There are no conflicts to declare.

Abbreviations

AlDMP	Aluminum tris(dimethylphosphate)
AlPi	Aluminum diethylephosphinate
APP	Ammonium polyphosphate
avEHC	Average effective heat of combustion
BaPL	Barrier and protective layer effect
CaDMP	Calcium bis(dimethylphosphate)
Ch	Charring effect
CY	Char yield
EDS	Energy dispersive X-ray spectroscopy
FI	Flame inhibition effect
FIGRA	Fire growth rate
FTIR	Fourier-transform infrared spectroscopy
G'	Storage modulus
G''	Loss modulus
G^*	Complex modulus
HRR	Heat release rate
iPP	Isotactic polypropylene
LOI	Limiting oxygen index
MHP	Melamine hypophosphite
MLC	Mass loss calorimeter
MP	Melamine phosphate
MPi	Melamine phosphite
MtDOP	Metal diorganophoshate
PBS	Poly(butylene succinate)
PER	Pentaerythritol
pHRR	Peak of heat release rate
PLA	Poly(lactic acid)
PPO	Poly(2,6-dimethyl-1,4-phenylene oxide)
SEM	Scanning electron microscope
ESI	Supplementary information
TEP	Triethyl phosphate
THE	Total heat evolved
TMP	Trimethyl phosphate
TPP	Triphenyl phosphate
TTI	Time to ignition
TTpHRR	Time to peak of heat release rate
ZnDMP	Zinc bis(dimethylphosphate)
δ	Loss angle
$\|\eta^*\|$	Complex viscosity
ω	Angular frequency

Data availability

Data supporting this study are openly available in the Mendeley Data Repository at https://doi.org/10.17632/c23m4hcrxd.1.

Supplementary information (SI): TGA–FTIR data of PBS and PBS/20%MtDOPs composites, SEM images of the cross-sections of the PBS/20%MtDOPs, additional SEM image of the internal structure of the Ca-containing solid residue, digital image of PBS/20%ZnDMP during burning in the MLC test, complex

viscosity curves recorded at different temperatures for PBS and its composites, Van Gurp–Palmen plots for PBS and PBS/20% MtDOPs, complex modulus variation in the low angular frequency region recorded at 190 °C, equations to calculate three main modes of action of MtDOPs as flame retardants, derivation of an equation governing the mean phosphorus concentration in volatile compounds, avEHC dependency of the average phosphorus concentration in volatiles. See DOI: https://doi.org/10.1039/d5ra06774j.

Acknowledgements

This research was partially funded by the National Science Centre, Poland within the OPUS-11 research scheme, grant number 2016/21/B/ST5/00126.

Notes and references

1 L. Aliotta, M. Seggiani, A. Lazzeri, V. Gigante and P. Cinelli, *Polymers*, 2022, **14**(4), 844.
2 J. Xu and B. Guo, *Biotechnol. J.*, 2010, **5**, 1149–1163.
3 F. Xiao, G. Fontaine and S. Bourbigot, *Polym. Degrad. Stab.*, 2021, **183**, 109466.
4 V. Rajgond, A. Mohite, N. More and A. More, *Polym. Bull.*, 2024, **81**, 5703–5752.
5 Y. Wang, F. Meng, J. Zhu, Z. Ba, D. Jiang, X. Wen and T. Tang, *Colloid Polym. Sci.*, 2023, **301**, 1529–1537.
6 Y. Wang, D. Jiang, X. Wen, T. Tang, K. Szymańska, K. Sielicki, K. Wenelska and E. Mijowska, *Front. Mater.*, 2021, **8**, 737749.
7 H. Yang, L. Song, Q. Tai, X. Wang, B. Yu, Y. Yuan, Y. Hu and R. K. K. Yuen, *Polym. Degrad. Stab.*, 2014, **105**, 248–256.
8 Y. Wang, C. Liu, J. Lai, C. Lu, X. Wu, Y. Cai, L. Gu, L. Yang, G. Zhang and G. Shi, *Polym. Test.*, 2020, **81**, 106174.
9 M. Kullas, M. Dębowski and K. Czaja, *Polym. Degrad. Stab.*, 2024, **221**, 110675.
10 H. Li, N. Ning, L. Zhang, Y. Wang, W. Liang and M. Tian, *Polym. Degrad. Stab.*, 2014, **105**, 86–95.
11 J. Andrzejewski and S. Michałowski, *Polymers*, 2022, **14**(19), 4086.
12 M. Dębowski, M. Kullas, K. Czaja, B. Sacher-Majewska, M. Bączek, M. Dranka, A. Ostrowski and Z. Florjańczyk, *Sci. Rep.*, 2025, **15**, 15447.
13 M. Dębowski, Z. Florjańczyk, K. Godlewska, A. Kaczmarczyk, M. Dranka and A. Ostrowski, *Polymers*, 2022, **14**(16), 3407.
14 M. Dębowski, K. Łokaj, A. Wolak, K. Żurawski, A. Plichta, J. Zachara, A. Ostrowski and Z. Florjańczyk, *Dalton Trans.*, 2016, **45**, 8008–8020.
15 M. Dębowski, K. Łokaj, A. Ostrowski, J. Zachara, P. Wiecińska, P. Falkowski, A. Krztoń-Maziopa and Z. Florjańczyk, *Dalton Trans.*, 2018, **47**, 16480–16491.
16 W. Zhang, J. Chen and H. Zeng, in *Polymer Science and Nanotechnology*, ed. R. Narain, Elsevier, 2020, ch. 8, pp. 149–178.
17 Introduction to Polymer Melt Rheology and its Application in Polymer Processing. https://www.tainstruments.com/pdf/literature/RH135.pdf, accessed 29 June 2025.
18 J. Aho, *PhD Thesis*, Tempere University of Technology, 2011.
19 B. K. Kandola, D. Price, G. J. Milnes and A. Da Silva, *Polym. Degrad. Stab.*, 2013, **98**(1), 52–63.
20 F. Kempel, B. Schartel, J. M. Marti, K. M. Butler, R. Rossi, S. R. Idelsohn, E. Oñate and A. Hofmann, *Fire Mater.*, 2015, **39**(6), 570–584.
21 A. Turski, S. Diniz, C. Huth and B. Schartel, *Polym. Degrad. Stab.*, 2020, **171**, 109048.
22 A. V. Shenoy, *Rheology of Filled Polymer Systems*, Springer Science+Business Media, Dodrecht, 1999.
23 L. A. Ultracki, *Polym. Compos.*, 1986, **7**(5), 274–282.
24 P. Pötschke, T. D. Fornes and D. R. Paul, *Polymer*, 2002, **43**(11), 3247–3255.
25 K. Taleb, S. Saidi-Besbes, I. Pillin and Y. Grohens, *ACS Omega*, 2022, **7**(47), 43254–43264.
26 T. C. Mokhena, E. R. Sadiku, S. S. Ray, M. J. Mochane and T. E. Motaung, *Polym. Compos.*, 2021, **42**(12), 6370–6382.
27 T. Kitano and T. Kataoka, *Rheol. Acta*, 1980, **19**, 753–763.
28 L. A. Ultracki, *Polym. Compos.*, 1986, **7**(5), 274–282.
29 Y. Jahani, *J. Vinyl Addit. Technol.*, 2010, **16**(1), 70–77.
30 S. Kashi, R. K. Gupta, T. Baum, N. Kao and S. N. Bhattacharya, *Composites, Part B*, 2018, **135**, 25–34.
31 A. Kelarakis and E. P. Giannelis, *Polymer*, 2011, **52**, 2221–2227.
32 L.-M. Yu and H.-X. Huang, *Polymer*, 2022, **247**, 124791.
33 B. Schartel and T. R. Hull, *Fire Mater.*, 2007, **31**(5), 327–354.
34 A. Rulmont, R. Cahay, M. Liegeois-Duyckaerts and P. Tarte, *Eur. J. Solid State Inorg. Chem.*, 1991, **28**, 207–219.
35 L. E. Jackson, B. M. Kriuki, M. E. Smith, J. E. Barralet and A. J. Wright, *Chem. Mater.*, 2005, **17**(18), 4642–4646.
36 J. M. Rojo, J. L. Mesa, L. Lezama and T. Rojo, *J. Mater. Chem.*, 1997, **7**, 2243–2248.
37 A. A. Dubale, W. N. Su, A. Tamirat, C. J. Pan, B. A. Aragaw, H. M. Chen, C. H. Chen and B. J. Hwang, *J. Mater. Chem. A*, 2014, **2**, 18383–18397.
38 I. Childres, L. A. Jauregui, W. Park, H. Cao and Y. P. Chen, in *New Developments in Photon and Materials Research*, ed. J. I. Jang, Nova Science Publishers, New York, 2013, Ch. 19, pp. 1–20.
39 H. J. Kim, S. M. Lee, Y. S. Oh, Y. H. Yang, Y. S. Lim, D. H. Yoon, C. Lee, J. Y. Kim and R. S. Ruoff, *Sci. Rep.*, 2014, **4**, 5176.
40 M. Molenda, A. Chojnacka, P. Natkański, E. Podstawka-Proniewicz, P. Kuśtrowski and R. Dziembaj, *J. Therm. Anal. Calorim.*, 2013, **113**, 329–334.
41 L. L. Velli, C. P. E. Varsamis, E. I. Kamitsos, D. Möncke and D. Ehrt, *Phys. Chem. Glasses*, 2005, **46**(2), 178–181.
42 S. Tang, V. Wachtendorf, P. Klack, L. Quian, Y. Dong and B. Schartel, *RSC Adv.*, 2017, **7**, 720–728.
43 S. Brehme, T. Köppl, B. Schartel and V. Altstädt, *e-Polym.*, 2014, **14**, 193–208.
44 B. Schartel, *Materials*, 2010, **3**(10), 4710–4745.
45 T. A. Bolshova, V. M. Shvartsberg, O. P. Korobeinichev and A. G. Shmakov, *Combust. Theory Model.*, 2016, **20**(2), 189–202.
46 E. D. Weil and S. V. Levchik, *Flame Retardants for Plastics and Textiles*, Carl Hanser Verlag GmbH & Co. KG, München, 2009.

47 T. M. Jayaweera, C. F. Melius, W. J. Pitz, C. K. Westbrook, O. P. Korobeinichev, V. M. Shvartsberg, A. G. Shmakov, I. V. Rybitskaya and H. J. Curran, *Combust. Flame*, 2005, **140**, 103–115.
48 I. Reva, A. Simão and R. Fausto, *Chem. Phys. Lett.*, 2005, **406**, 126–136.
49 C. Hu, S. Bourbigot and G. Fontaine, *Polym. Degrad. Stab.*, 2025, **236**, 111318.
50 A. Dwivedi, V. Baboo, A. Bajpai and J. Theoret, *Chem*, 2015, **2015**, 345234.
51 S. Rabe, Y. Chuenban and B. Schartel, *Materials*, 2017, **10**(5), 455.
52 S. Brehme, T. Köppl, B. Schartel and V. Altstädt, *e-Polym.*, 2014, **14**, 193–208.
53 G. F. Levchik, S. V. Levchik, G. Camino and E. D. Weil, Fire retardant action of red phosphorus in Nylon 6, in *Fire Retardancy of Polymers the Use of Intumescence*, ed. M. Le Bras, G. Camino, S. Bourbigot and R. Delobel, Special Publication–Royal Society of Chemistry, 1998, vol. 224, pp. 304–315.
54 O. P. Korobeinichev, V. M. Shwartsberg, A. G. Shmakov, D. A. Knyazkov and I. V. Rybitskaya, *Proc. Combust. Inst.*, 2007, **31**, 2741–2748.
55 E. D. Weil, M. Hirschler, N. G. Patel, M. M. Said and S. Shakir, *Fire Mater.*, 1992, **16**(4), 159–167.
56 W. Tao, X. Hu, J. Sun, L. Quian and J. Li, *Polym. Degrad. Stab.*, 2020, **174**, 109092.
57 B. Schartel, M. Bartholmai and U. Knoll, *Polym. Degrad. Stab.*, 2005, **88**, 540–547.
58 Y. Yu, L. Xi, M. Yao, L. Liu, Y. Zhang, S. Huo, Z. Fang and P. Song, *iScience*, 2022, **25**(3), 103950.
59 P. R. Johnson, *J. Appl. Polym. Sci.*, 1974, **18**(2), 491–504.
60 B. Schartel, R. Kunze and D. Neubert, *J. Appl. Polym. Sci.*, 2022, **7**, 2060–2071.
61 R. Chen, S. Lu, S. Li, Y. B. Zhang and S. Lo, *J. Therm. Anal. Calorim.*, 2016, **123**, 545–556.